NATIONAL AERONAUTICS AND SPACE ADMINISTRATION

TECHNICAL MEMORANDUM X-599

EXPERIMENTAL INVESTIGATION OF THE TRANSONIC FLUTTER OF SIMPLE THIN TRUNCATED-CONE PANELS*

By Jean Gilman, Jr.

SUMMARY

An experimental investigation has been conducted at stream Mach numbers near 0.8, 1.0, and 1.2 to determine the effects of variations in panel differential pressure and dynamic pressure on the transonic flutter characteristics of simple thin aluminum panels contoured to form a segment of a conical surface. The two panel configurations tested, in which all edges were restrained, had length-to-thickness ratios of about 2,400 and 1,200. Panel external pressure distribution varied with Mach number and dynamic pressure.

When the pressure in the compartment behind the panel was reduced sufficiently below the maximum external pressure to cause buckling, the panels experienced random vibrations or fluttered. The reduction in compartment pressure below maximum external pressure required to destabilize the panels, although in general small, became greater as the panel thickness or dynamic pressure was increased. Neither random vibrations nor flutter were immediately destructive.

INTRODUCTION

Designs of ballistic and space vehicles frequently require the use of large thin panels in the form of truncated-cone segments located, for example, near the nose. Such panels may be subject to panel flutter, particularly in the transonic region of the launch trajectory where high dynamic pressures are usually encountered. Most of the published works on panel flutter (largely summarized in ref. 1) deal with the flutter of flat plates or cylindrical shells in various configurations. A more recent work (ref. 2) presents representative experimental results that give design criteria incorporating the effects of various quantities

*Title, Unclassified.

such as Mach number, differential pressure, and aerodynamic heating on the flutter of unstiffened and stiffened rectangular flat plates. Reference 3 presents some experimental data for buckled stiffened cylindrical-segment panels at transonic and supersonic speeds. A theoretical study of flutter of truncated cones at supersonic speeds has been reported in reference 4. There appears to be no proven theoretical method and very little experimental data for dealing with the problem of conical segments at transonic speeds.

In view of the lack of transonic flutter data for thin panels on conical surfaces, a brief experimental investigation of simple thin panels of this type has been conducted in the Langley 8-foot transonic pressure tunnel. Effects of variations in both panel differential pressure and stream dynamic pressure on panel stability were investigated at stream Mach numbers near 0.8, 1.0, and 1.2 for two panel thicknesses.

L 5 8 4

SYMBOLS

c_p	local pressure coefficient, $\frac{p_l - p}{q}$
$c_{p,max}$	maximum local pressure coefficient on panel, $\frac{p_{max} - p}{q}$
E	Young's modulus, lb/sq in.
f	frequency, cps
l	unsupported panel length, in.
M	Mach number of stream
M_l	local Mach number
p	static pressure of airstream, lb/sq ft
p_c	compartment pressure, lb/sq ft
p_l	local static pressure, lb/sq ft
p_{max}	maximum external static pressure on panel, lb/sq ft
q	dynamic pressure, $\frac{1}{2}\rho V^2$, lb/sq ft
t	panel thickness, in.

V stream velocity, ft/sec

$\beta = \sqrt{M^2 - 1}$

Δp panel differential pressure, $p_c - p_{max}$, lb/sq ft

Δp_l panel local differential pressure, $p_c - p_l$, lb/sq ft

ρ density of air, slugs/cu ft

APPARATUS AND METHODS

Models

Figure 1 is a composite sketch of the forward portion of a missile nose having one or more panels located on a conical surface, with a superimposed view (solid lines) of a smaller symmetrical body derived from the nose shape which preserves a portion of the conical surface in the region of one of the panels. A test body similar to the superimposed body of figure 1, modified by rounding the sharp edges at the juncture of the two halves as shown by the detailed sketch in figure 2, was constructed in accordance with original plans to conduct the present investigation in a small blowdown wind tunnel. Because of a lack of control of the airstream temperature, testing in the small tunnel later proved to be impractical. Figure 3 is a photograph of the model.

Panels tested were of 0.002-inch- and 0.004-inch-thick aluminum (ratios of developed length to thickness of about 2,400 and 1,200, respectively) and were bonded on all four edges. Details of the panel-mounting frame are shown in figure 4. Figure 5 is a photograph of a bare frame and of a frame with a panel attached. Principal panel exposed dimensions other than thickness are given in table I.

Care was taken to avoid wrinkling or buckling the panels in the bonding process, and since no edge restraints were used during the cement-curing period, it is believed that initial tensile forces on the panels were uniformly low. In view of tensile-force effectiveness in raising the flutter q (as shown, for example, in ref. 5) it was, of course, thought advisable in the present tests to keep initial tensile forces low in an effort to define lower limits of the flutter boundary.

The panel assembly was installed in a receptacle in the test body (fig. 2) on a gasket and was bolted in place to form an airtight inner compartment. This compartment was vented to a plenum chamber, the

pressure in which was controllable to provide variable panel pressure differential during the tests. Gaps between the edges of the panel frame and the body surface were filled with a rubber compound to form a smooth external surface. To highlight panel motions during the tests, the panels were spray-painted with a thin coat of flat white enamel in such a manner as to form a grid of bare metal (figs. 3 and 5).

A dummy panel containing orifices for performing local pressure measurements in the panel region was constructed for the tests. An additional orifice was installed ahead of the panel; the location of the pressure survey orifices is shown in figure 6.

Instrumentation

Four induction coils, installed as shown in figure 7, were used to detect panel displacements. The gap between these gages and the inner panel surface was about 1/4 inch. Gages 1 and 2 were located at $\frac{1}{4}l$ and $\frac{3}{4}l$, respectively, along the panel longitudinal center line. Gages 3 and 4 were placed on the panel lateral center line at 2/3 local semispan on opposite sides of the longitudinal center line. Tunnel stagnation pressure, static pressure, panel compartment pressure, and local pressures were measured with electrical pressure transducers. The transducer and displacement coil outputs were continuously recorded by oscillograph equipment. Because of the duration of a test run, approximately 20 minutes, the oscillograph could not be operated continuously at paper speeds sufficiently high to determine frequency content. Hence the dynamic components of the induction coil outputs were also continuously recorded on magnetic tape for subsequent frequency analysis of the significant portions of the runs. Time correlation of the magnetic tape records and oscillograph records was accomplished with an electrical timing device. Tunnel stagnation temperature was continuously recorded by a potentiometer-type instrument. Two high-speed motion-picture cameras operating at approximately 1,000 frames per second and one motion-picture camera operating at 12 frames per second were used in an effort to obtain motion pictures of panel oscillations. In addition to the foregoing recorded information, displacement coil outputs were monitored with an oscilloscope during the runs as a guide to panel activity. Visual observation of the panels required the use of a telescope. Compartment pressure was monitored by means of a liquid manometer.

Tests

Wind-tunnel characteristics.- Upper and lower limits of stream dynamic pressure attainable in the transonic Mach number range of the

Langley 8-foot transonic pressure tunnel are shown in figure 8. The wind-tunnel air-conditioning equipment provides control of the stagnation temperature through a limited temperature range; for the present tests, the stagnation temperature was held constant at 120° F.

Test procedure.- The test procedure, carried out at a body angle of attack of 0°, consisted of maintaining a panel compartment pressure sufficiently high to stabilize the panel during the period required to bring the airstream to a desired Mach number and dynamic pressure. Upon reaching desired airstream conditions, the recording equipment was put into operation, and the compartment pressure was reduced until the panel reached a vibratory state. In an effort to obtain adequate vibration records, the compartment pressure was usually further reduced by about 15 to 30 lb/sq ft (about 0.1 to 0.2 lb/sq in.) to increase the vibration amplitude. Compartment pressure was then increased to restabilize the panel, and if the panel appeared undamaged, the testing procedure was repeated at an increased dynamic pressure. Damaged panels were replaced.

The low-speed motion-picture camera was run continuously during most of the runs. The combined duration of both high-speed cameras, however, was only about 30 seconds and they were inaccessible for reloading during a run. This short duration combined with occasional camera malfunctioning contributed to a rather incomplete photographic coverage of the tests. The high-speed cameras were operated in short bursts (usual duration, about 2 seconds) during the panel vibratory state.

Pressure-distribution measurements.- Prior to the flutter tests the dummy orifice panel was fitted into the test body to obtain pressure-distribution measurements. Local pressures referred to the stream static pressure were measured at a body angle of attack of 0° through the tunnel Mach number range. Stream stagnation pressure was held approximately constant near a value of 1 atmosphere.

Accuracy

The frequency response of the recording equipment was flat up to 1,500 cps. The amplitude response of an induction coil, however, is linear over only a very small range which was probably exceeded in the tests. Pressure measurements made with the electrical transducers were accurate to about ±0.05 lb/sq in. (about 7.5 lb/sq ft). Panel thicknesses quoted are for commercial-grade aluminum sheets; thickness deviations were too small to be detected with an ordinary machinist's micrometer.

RESULTS AND DISCUSSION

Presentation of Results

Pressure distribution.- Local pressure coefficients c_p derived from the pressure-distribution measurements are given in table II. Associated values of local Mach number M_l are given in table III. Distributions of local pressure coefficient and Mach number along the body longitudinal center line (stations 1 to 4) are shown plotted in figures 9 and 10, respectively. In table II if the local pressure coefficients obtained at the panel 2/3 local semispan stations (stations 5 to 7, fig. 6) are compared with those obtained along the panel center line (stations 2 to 4), the local spanwise pressure distribution is essentially uniform for the first two pairs of orifices. For the rearward pair at stations 4 and 7, however, the pressure coefficients near the panel edge are about 0.03 lower than the values at the panel center line. The corresponding difference in spanwise local Mach number is about 0.02 at the rearward stations. (See table III.)

The chordwise pressure gradient in figure 9 is seen to be of negative slope at all Mach numbers from 0.7 to 1.2. The slope tends to become less negative at Mach numbers above about 1.1. Shown in figure 11 are pressure distributions along the side of various conical nose configurations for comparison with the distributions of the present body, all at an angle of attack of 0°. Included are some unpublished data for a blunt body of revolution as in figure 1, data from reference 6 on a 14.45° semiangle spherical-tipped cone, and data from reference 7 on a sharp-tipped 10° semiangle cone. At a Mach number of 0.8, the pressure gradient of the present body in general lies between the gradients of the other bodies; at Mach number 1.0, the gradient is steeper than those for either of the cones; and at Mach number 1.2, the cone pressure gradients over most of the body are flat. The pressure gradient of the blunt body of revolution, although nearly of the same slope, is opposite to that of the body used in the experiments.

The external pressure gradients exhibited in figure 9 make the definition of panel differential pressure a matter of interpretation. In the present paper, for a reason which will appear later, the pressure difference is defined as $\Delta p = p_c - p_{max}$, that is, compartment pressure minus the maximum local external pressure (in the present tests, this maximum pressure occurs at the leading edge of the exposed panel, fig. 9).

The value of p_{max} was obtained for a given airstream condition by means of a cross plot of the pressure coefficient at the panel leading

edge as a function of Mach number. Comparison at a given Mach number of the local pressure coefficient ahead of the panel (station 1, fig. 6) obtained during the panel tests at varying stagnation pressures with the values obtained from the pressure survey at a fixed stagnation pressure of about 1 atmosphere indicated little dependence of pressure coefficient on stagnation pressure within the range of the tests.

Panel test data.- The test runs made, the panels tested, panel thicknesses, airstream characteristics, values of panel differential pressure Δp, and values of flutter motion frequencies or range of predominant frequencies of random motions are given in table IV. Results are shown plotted for the 0.002-inch- and the 0.004-inch-thick panels in figures 12 and 13, respectively. Excerpts from the motion pictures to help visualize the panel activity are shown in figures 14 to 16. Associated frequency modes from the magnetic tape recordings are given in figures 17 to 19.

Throughout table IV, in general, the panel instability characterized by point B (start of buckling and random vibrations), initiated by reducing the panel differential pressure from a stable value to the values tabulated, consisted of the simultaneous formation of a buckle and start of random vibrations. A further reduction in differential pressure served to increase the buckled area and also to increase the vibration amplitude. The buckling mode consisted of either a single buckle as in figure 14 or a multiple buckle as in figure 15. There appeared to be no set pattern as to which type might occur; for example, in two consecutive runs near $M = 0.8$, model 4 experienced a single buckle at $q = 352$ lb/sq ft (run 8) and a multiple buckle at $q = 532$ lb/sq ft (run 9).

When the single buckle occurred, the forward chordwise displacement gage under the buckled region (gage 1) and the nearby spanwise gages (gages 3 and 4) showed a varying amplitude frequency response as in figure 17. The rearward chordwise gage (gage 2) showed a lesser response. For the multiple buckle, characterized by one or more chordwise ridges near the panel center line, gages 1 and 2 under the ridge, or ridges, showed little response (fig. 18), whereas spanwise gages 3 and 4 under the collapsed portions of the panel showed a varying amplitude-frequency response.

Flutter (data denoted by F in table IV), which in the present investigation occurred at Mach numbers near 1.2 only, involved a general flattening of the panel. This general flattening was more extensive in area than the previously described buckles. As will be more fully discussed, this more general collapse was associated with the flatter external pressure gradient at Mach number 1.2 (fig. 9). The flattened appearance of the panel can be seen in figure 16. The associated frequency response (fig. 19) is harmonic.

The values of Δp and the levels of dynamic pressure at which the events just described occurred are shown in figures 12 and 13 for 0.002-inch- and 0.004-inch-thick panels, respectively. Also, shown are the lowest value of Δp during a run, the value required to restabilize a panel, or the destruction of a panel (data denoted by L, E, or X, respectively, table IV).

Although figures 12 and 13 give an overall view of the test range and panel activity, the sequence of events during a run can be more easily followed in table IV. Take, for example, the activity of model 1 (0.002-inch-thick panel) during run 1, the panel buckled and became dynamically unstable at $\Delta p = -1.0$ lb/sq ft (point B in table IV and circular test points in fig. 12(a)). The point L in table IV (triangular test points in fig. 12(a)) shows that the lowest Δp during the run was -24.5 lb/sq ft. The point E (diamond-shaped test points in fig. 12(a)) defines the value of Δp, -3.0 lb/sq ft, at which the panel was restabilized at the end of the run. Predominant frequencies during the unstable period lay in the range between 300 and 400 cycles per second. During run 1, the unintended change in Mach number (0.783 to 0.805) and dynamic pressure (317 lb/sq ft to 327 lb/sq ft) was larger than the change for subsequent runs.

For model 3 (0.002-inch-thick panel, table IV) the sequence of events during run 6 was more varied. Flutter at 120 cps commenced at $\Delta p = -6.0$ lb/sq ft. An imperceptible reduction in Δp, during the process of which the flutter frequency increased to 145 cps, changed the vibratory mode from one of flutter to one of random motion. During the period in which Δp was reduced to the lowest value of the run, -27.0 lb/sq ft, and increased to -17.0 lb/sq ft, the random frequencies lay in the range from 300 to 500 cps. At $\Delta p = -17.0$ lb/sq ft the vibratory mode again became harmonic at 257 cps; the flutter frequency gradually reduced to 200 cps as Δp approached 3.0 lb/sq ft. At this latter value of Δp the model became statically and dynamically stable.

In run 7 at a higher value of dynamic pressure, model 3 commenced fluttering at $\Delta p = -1.0$ lb/sq ft. At $\Delta p = -5.0$ lb/sq ft the model was seen from the slow-speed motion pictures to have failed at the trailing edge. During this sequence the flutter frequency increased from 210 cps at the start to 250 cps at the point of failure.

In run 9 with model 4 (0.004-inch-thick panel, table IV), Δp was inadvertently reduced to such a low value that the inward collapse of the panel destroyed the edge bonding. The oscillograph recording paper was exhausted prior to this event so that the value of Δp could not be ascertained.

Flutter of the 0.004-inch-thick panel (model 8, run 25, table IV) was very mild compared to the flutter of the thinner panel. As shown

in the table, this flutter commenced at the lowest value of Δp during the run, -56.0 lb/sq ft, and continued at a constant frequency of 160 cps until the panel was restabilized at Δp = -26.0 lb/sq ft. The value of dynamic pressure, 882 lb/sq ft, is near the maximum attainable in the wind tunnel at Mach number 1.2 (fig. 8).

Attempts to obtain high-speed motion pictures of flutter were unsuccessful because of difficulty in observing the model during tests. The flutter mode, standing wave or traveling wave, is therefore not known. Neither flutter nor random vibrations were immediately destructive; the 0.002-inch-thick panel (model 3, runs 6 and 7, table IV) failed at the trailing edge because of flutter at Mach number 1.2 but only after a large number of oscillations. This model fluttered initially near the lowest dynamic pressure attainable in the wind tunnel; hence, the flutter boundary is not defined.

The dynamic-pressure range of the tests at $M = 0.8$ is unfortunately small; the tests at this Mach number were conducted early in the investigation, before an adequate appreciation was gained of the compartment pressure required to prevent buckling. A number of panels were lost before reaching desired airstream conditions. As explained in the section "Tests," the recording equipment was not in operation during these periods; hence, no data were obtained on these early failures.

Discussion of Results

Differential pressure required to buckle panels.- Results for the 0.002-inch-thick panels in figure 12 show that initial panel instability (circular test points) occurred near the point where the compartment pressure was reduced to a value approximately equal to the maximum external pressure on the panel ($\Delta p = 0$). For the 0.004-inch-thick panels of figure 13 a somewhat larger reduction in compartment pressure (more negative value of Δp) was necessary to produce instability. No instability occurred throughout the dynamic-pressure and Mach number ranges of the tests as long as p_c was greater than p_{max} ($\Delta p > 0$).

Motion-picture studies indicated that, in general, panel vibrations were coincident with the formation of a buckle; thus, a relation is implied between the dynamic instability of a thin curved panel and the static instability or collapsing strength. For all conditions where Δp was high enough to prevent static instability (buckling) no dynamic instability occurred. Since the panels buckled near $\Delta p = 0$, the static instability point for membranes, it appears that membrane behavior has a dominant effect on the stiffness of these thin panels. The structural rigidity, which is proportional to the cube of the panel thickness, of the present curved panels is so small that their ability to resist buckling is highly dependent on membrane-type stiffness, which is

proportional to the panel tensile force, which is in turn governed by the differential pressure. The fact that, when $p_c = p_{max}$, small pressure perturbations will cause deformations (buckles) on a curved membrane points to p_{max} as a primary choice to use in defining Δp. It will appear from the discussion in the next section, however, that values of Δp required to produce buckling of structural panels vary in a complex manner.

A further inspection of the data in figures 12 and 13 reveals that a higher compartment pressure is usually required to restabilize a panel than to initially destabilize it (diamond-shaped test points). This feature may not be particularly significant since design effort would be logically directed toward avoiding the initial destabilization.

Effect of pressure gradient.- A noticeable feature of the results in figure 13(b) is a trend in which initial panel instability occurs at progressively more negative values of Δp as dynamic pressure increases. This trend is attributed, at least in part, to the effect of differential pressure-distribution variations on panel stiffness as indicated by the following qualitative consideration.

Local differential pressures vary in accordance with the relation

$$\Delta p_l = \Delta p + (c_{p,max} - c_p)q$$

Since the quantity $c_{p,max} - c_p$ is greater than or equal to 0 and is fixed with Mach number (fig. 9), it is evident that, where nonzero pressure gradients exist, the values of Δp_l become increasingly greater than Δp as q increases. For example, shown in figure 20 are distributions of Δp_l along the panel longitudinal center line for two cases having the same value of Δp, one of which produces panel instability and another wherein the panel is within the stable range (fig. 13(b)). The increases in Δp_l with increased q at constant M are readily apparent. For the case of initial panel instability at the lower q it is seen that, although positive differential pressures which act to stabilize the panel exist over the rearward portion, differential pressures on a relatively large area of the forward portion are negative and are acting to collapse the panel. At the higher q and for the same differential pressure at the leading edge, $\Delta p = -24$ lb/sq ft, Δp_l values have increased and are stabilizing over most of the panel area. The panel is well within the stable region (fig. 13(b)); thus, it is evident that under certain conditions the effect of relatively steep pressure gradients - for example, at Mach number 1 in the present tests - is to produce an increase in panel stability as q increases. Hence initial instability occurs at

compensatingly lower values of Δp; at the higher level of q in figure 20, for example, the instability occurs at $\Delta p = -62$ lb/sq ft in contrast to -24 lb/sq ft at the lower level of q.

On examining the results at $M = 1.2$ (fig. 13(c)), it is seen that the trend just cited is much less pronounced than at $M = 1.0$ (fig. 13(b)). Likewise, the pressure coefficient gradient at $M = 1.2$ is considerably less than at $M = 1.0$. (See fig. 9.) Values of $(c_{p,max} - c_p)$ are accordingly reduced; hence the increases in Δp_l caused by increasing q at fixed Δp and the attendant increases in stability are less pronounced at the supersonic Mach number. Therefore, as q increases, the compensatory reductions in Δp required to allow buckling are less evident at Mach number 1.2 than at Mach number 1.0.

In addition the motion pictures showed that initial buckling involved a more extensive area of the panel at Mach number 1.2 than at either Mach number 1.0 or 0.8, as would be expected when the lesser pressure gradient at Mach number 1.2 is considered. In view of the more severe vibration problem (flutter as contrasted to less-violent random vibrations) associated with the lesser pressure gradient at $M = 1.2$, there remains a question as to the effect of reduced or zero pressure gradient on the results of the present investigation. Inasmuch as flow fields of this latter type could be possibly encountered in practice (with the present body, for example, at some angle of attack other than zero), it appears that future investigations of similar panel flutter problems should include this probably more severe case. It is probable that panels of the present type, if tested in a flow field of near-zero pressure gradient, would require slightly higher than the present values of Δp for marginal stability, and that initial buckling would involve a larger area of the panel. The present results should therefore be interpreted with caution.

Comparison of flutter data.- As has been previously mentioned, flutter of the 0.002-inch-thick panel occurred at the lowest dynamic pressure attainable in the wind tunnel, so the flutter boundary has not been defined. For the 0.004-inch-thick panel, however, flutter was encountered at a dynamic pressure of 882 lb/sq ft (table IV, run 25, $M = 1.2$). At the next lower level of dynamic pressure, 708 lb/sq ft, run 24, random oscillations were encountered. Resulting values of the flutter parameter $\frac{t}{l}\left(\frac{E}{q}\beta\right)^{1/3}$ (ref. 3) are 0.085 and 0.092, respectively. The flutter boundary lies between these two values. In flutter tests of circular arc panels in various configurations (flow along the generatrix, ref. 3), the value of this parameter at a Mach number of 1.3 was found to range from 0.08 to 0.10; the present results are in the same range.

If comparisons are made with the flutter criteria presented in reference 2, the value of the flutter parameter is found to be approximately 0.47 for a panel length-to-width ratio of 1.3; thus, the criteria of reference 2, which are based mainly on flat panel tests, indicate that a much higher value of $\frac{t}{l}\left(\frac{E\beta}{q}\right)^{1/3}$ is required to prevent flutter than was found in the present tests or in those of reference 3. The reasons for this difference are not clearly understood; however, it may be surmised that the effects of curvature and relatively high pressure gradients may be beneficial in the prevention of panel flutter.

CONCLUSIONS

An experimental investigation has been conducted at stream Mach numbers near 0.8, 1.0, and 1.2 to determine the effects of changes in panel differential pressure and dynamic pressure on the dynamic stability of simple thin aluminum panels which were contoured to form a truncated-cone-segment shape. Two thicknesses of panels were tested with all edges restrained. Initial panel tensile forces are believed to have been small because of the method used in bonding the edges. Panel external pressure distribution varied with Mach number and dynamic pressure. This investigation has indicated the following conclusions:

1. When the pressure in the compartment behind the panel was reduced sufficiently below the maximum external pressure to cause buckling, the panels experienced random vibrations or fluttered.

2. The reduction in compartment pressure below maximum external pressure required to destabilize the panels, although in general small, became greater as panel thickness or dynamic pressure was increased.

3. Neither random vibrations nor flutter were immediately destructive.

Langley Research Center,
National Aeronautics and Space Administration,
Langley Air Force Base, Va., July 26, 1961.

REFERENCES

1. Fung, Y. C. B.: A Summary of the Theories and Experiments on Panel Flutter. AFOSR TN 60-224, Guggenheim Aero. Lab., C.I.T., May 1960.

2. Kordes, Eldon E., Tuovila, Weimer J., and Guy, Lawrence D.: Flutter Research on Skin Panels. NASA TN D-451, 1960.

3. Tuovila, W. J., and Hess, Robert W.: Experimental Investigation of Flutter of Buckled Curved Panels Having Longitudinal Stringers at Transonic and Supersonic Speeds. NASA MEMO 5-18-59L, 1959.

4. Shulman, Yechiel: Vibration and Flutter of Cylindrical and Conical Shells. ASRL Tech. Rep. No. 74-2 (OSR Tech. Rep. 59-776), M.I.T., June 1959.

5. Hedgepeth, John M.: Flutter of Rectangular Simply Supported Panels at High Supersonic Speeds. Jour. Aero. Sci., vol. 24, no. 8, Aug. 1957, pp. 563-573, 586.

6. Coe, Charles F.: Steady and Fluctuating Pressures at Transonic Speeds on Two Space-Vehicle Payload Shapes. NASA TM X-503, 1961.

7. Estabrooks, Bruce B.: Wall-Interference Effects on Axisymmetric Bodies in Transonic Wind Tunnels With Perforated Wall Test Sections. AEDC-TR-59-12, ASTIA Doc. No.: AD-216698 (Contract No. AF 40(600)-700 S/A 13(59-1)), Arnold Eng. Dev. Center, June 1959.

[redacted]

TABLE I.- PANEL DIMENSIONS

Developed length, in.	4.832
Projected length, in.	4.750
Leading-edge width, in.	3.344
Trailing-edge width, in.	4.094
Leading-edge radius, in.	4.993
Trailing-edge radius, in.	5.882
Developed panel area, sq in.	18.68
Slope of panel longitudinal center line, deg	10.93

TABLE II.- LOCAL PRESSURE COEFFICIENTS

M	c_p at station[a] -						
	1	2	3	4	5	6	7
0.70	0.162	0.065	-0.025	-0.166	0.059	-0.025	-0.185
.80	.176	.079	-.013	-.151	.074	-.014	-.179
.85	.191	.094	.003	-.127	.088	.001	-.157
.90	.213	.118	.032	-.090	.112	.031	-.119
.95	.249	.157	.079	-.033	.155	.080	-.063
1.00	.292	.205	.131	.026	.200	.130	-.001
1.05	.357	.270	.199	.097	.266	.199	.071
1.10	.352	.284	.226	.137	.279	.226	.112
1.15	.321	.267	.226	.152	.266	.227	.130
1.20	.291	.246	.215	.169	.241	.215	.145

[a]See figure 6.

TABLE III.- LOCAL MACH NUMBERS

M	M_l at station[a] -						
	1	2	3	4	5	6	7
0.8	0.725	0.768	0.809	0.871	0.771	0.809	0.885
.9	.795	.845	.888	.952	.846	.890	.968
1.0	.835	.885	.927	.989	.888	.927	1.005
1.1	.880	.922	.959	1.015	.924	.959	1.032
1.2	.992	1.023	1.043	1.077	1.026	1.043	1.094

[a]See figure 6.

TABLE IV.- SUMMARY OF PANEL TEST RESULTS

Model	Panel thickness, t, in.	Run	Point (chronological order) (a)	Mach number, M	Dynamic pressure, q, lb/sq ft	Stream velocity, V, ft/sec	Air density, ρ, slugs/cu ft	Pressure differential, Δp, lb/sq ft	Panel frequency, f, cps (b)
1	0.002	1	B	0.783	317	872.1	0.00083	-1.0	300 to 400
			L	.805	327	893.8	.00082	-24.5	
			E	.805	327	893.8	.00082	-3.0	
2	.002	2	B	.988	184	1,066.5	.00032	-7.0	250 to 400
			L	.990	186	1,068.2	.00033	-12.0	
			E	.990	186	1,068.2	.00033	-7.0	
		3	B	1.008	335	1,084.4	.00057	-13.0	250 to 400
			L	1.004	332	1,080.8	.00057	-21.0	
			E	1.004	332	1,080.8	.00057	-7.0	
		4	B	1.002	478	1,079.0	.00082	-17.0	300
			L	1.003	481	1,079.9	.00082	-26.0	
			E	1.003	481	1,079.9	.00082	-11.0	
		5	B	1.009	630	1,085.3	.00107	-20.0	250
			L	1.010	629	1,086.2	.00107	-28.0	
			E	1.010	629	1,086.2	.00107	-3.0	
3	.002	6	F	1.186	207	1,236.4	.00027	-6.0	120
			E	1.186	207	1,236.4	.00027	-6.0	145
			B	1.186	207	1,236.4	.00027	-6.0	300 to 500
			L	1.186	207	1,236.4	.00027	-27.0	
			F	1.186	207	1,236.4	.00027	-17.0	257
			E	1.186	207	1,236.4	.00027	+3.0	200
		7	F	1.201	373	1,248.5	.00048	-1.0	210
			X	1.199	374	1,247.0	.00048	-5.0	250
4	.004	8	B	.797	352	885.9	.00090	-45.0	250 to 300
			L	.794	351	882.9	.00090	-47.0	
			E	.794	351	882.9	.00090	-23.0	
		9	B	.804	532	892.8	.00133	-46	300 to 400
			X	.810	533	898.7	.00132		
5	.004	10	B	.987	232	1,065.5	.00041	-17.0	300 to 400
			L	.971	232	1,051.0	.00042	-54.0	
			E	.987	232	1,065.5	.00041	-21.0	
		11	B	1.001	368	1,078.1	.00063	-46.0	200 to 400
			L	1.001	368	1,078.1	.00063	-117.0	
			E	1.001	368	1,078.1	.00063	-14.0	
		12	B	1.003	514	1,079.9	.00088	-31.0	250
			L	1.003	514	1,079.9	.00088	-46.0	
			E	1.003	514	1,079.9	.00088	+4.6	

[a]Point identification key:
- B Start of buckling and random vibrations
- F Start of flutter
- E End of buckling and random vibrations or flutter
- L Lowest compartment-panel pressure difference during run
- X Model destroyed

[b]Frequencies given for points designated B are the predominant frequency or frequency range. The response is random and nonharmonic. Frequency responses for flutter points (F) are harmonic.

TABLE IV.- SUMMARY OF PANEL TEST RESULTS - Concluded

Model	Panel thickness, t, in.	Run	Point (chronological order) (a)	Mach number, M	Dynamic pressure, q, lb/sq ft	Stream velocity, V, ft/sec	Air density, ρ, slugs/cu ft	Pressure differential, Δp, lb/sq ft	Panel frequency, f, cps (b)
6	0.004	13	B	0.994	518	1,071.9	0.00090	-39.0	250
			L	.995	518	1,072.7	.00090	-53.0	
			E	.995	518	1,072.7	.00090	-38.0	
		14	B	1.011	668	1,087.2	.00113	-59.0	200 to 250
			L	1.010	667	1,086.2	.00113	-60	
			E	1.010	667	1,086.2	.00113	-35.0	
		15	B	1.007	818	1,083.5	.00139	-62.0	250
			L	1.007	818	1,083.5	.00139	-70.0	
			E	1.007	818	1,083.5	.00139	-43.0	
		16	B	1.008	976	1,084.4	.00166	-71.0	250 to 400
			L	1.008	976	1,084.4	.00166	-85.0	
			E	1.006	974	1,082.7	.00166	-39.0	
		17	B	1.007	1,121	1,083.5	.00191	-82.0	250 to 400
			L	1.007	1,120	1,083.5	.00191	-96.0	
			E	1.007	1,120	1,083.5	.00191	-49.0	
7	.004	18	B	1.000	184	1,077.2	.00032	-24.0	250 to 400
			L	.999	184	1,076.4	.00032	-29.0	
			E	.999	184	1,076.4	.00032	-24.0	
		19	B	1.004	334	1,080.9	.00057	-38.0	250 to 350
			L	1.007	333	1,083.5	.00057	-44.0	
			E	1.007	333	1,083.5	.00057	-34.0	
		20	B	1.007	483	1,083.5	.00082	-55.0	250 to 350
			E	1.007	483	1,083.5	.00082	-22.0	
8	.004	21	B	1.183	208	1,234.0	.00027	-11.0	400
			L	1.180	207	1,231.6	.00027	-79.0	
			E	1.180	207	1,231.6	.00027	-8.0	
		22	B	1.195	371	1,243.8	.00048	-9.0	350 to 400
			L	1.194	374	1,242.9	.00048	-28.0	
		23	B	1.197	541	1,245.3	.00070	-12.0	400
			L	1.201	540	1,248.5	.00069	-30.0	
			E	1.201	540	1,248.5	.00069	-27.0	
		24	B	1.203	708	1,250.2	.00090	-23.0	400
			L	1.203	706	1,250.2	.00090	-31.0	
			E	1.203	706	1,250.2	.00090	-28.0	
		25	B	1.202	882	1,249.4	.00113	-26.0	400
			L	1.203	882	1,250.2	.00113	-56.0	
			F	1.203	882	1,250.2	.00113	-56.0	160
			E	1.203	882	1,250.2	.00113	-26.0	

[a]Point identification key:

B Start of buckling and random vibrations
F Start of flutter
E End of buckling and random vibrations or flutter
L Lowest compartment-panel pressure difference during run
X Model destroyed

[b]Frequencies given for points designated B are the predominant frequency or frequency range. The response is random and nonharmonic. Frequency responses for flutter points (F) are harmonic.

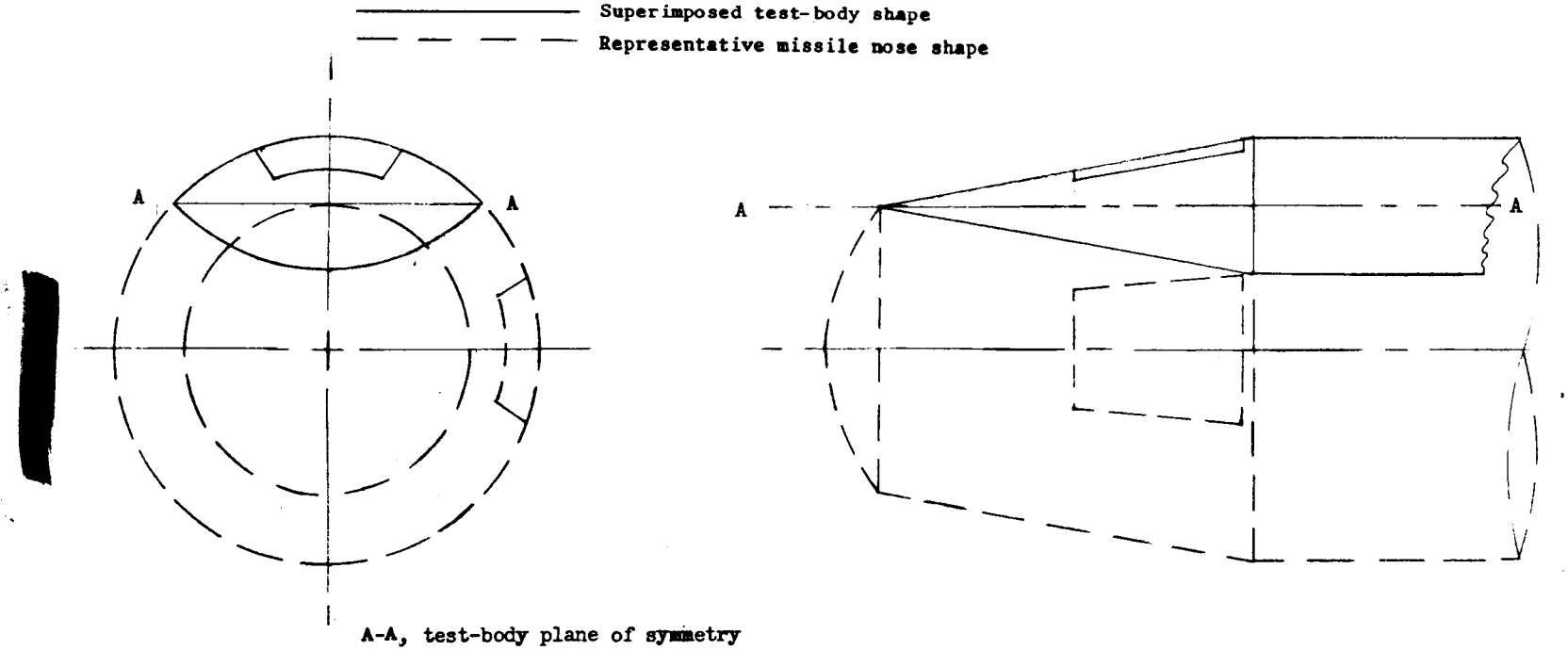

Figure 1.- Relation of test body and panel to representative nose configuration.

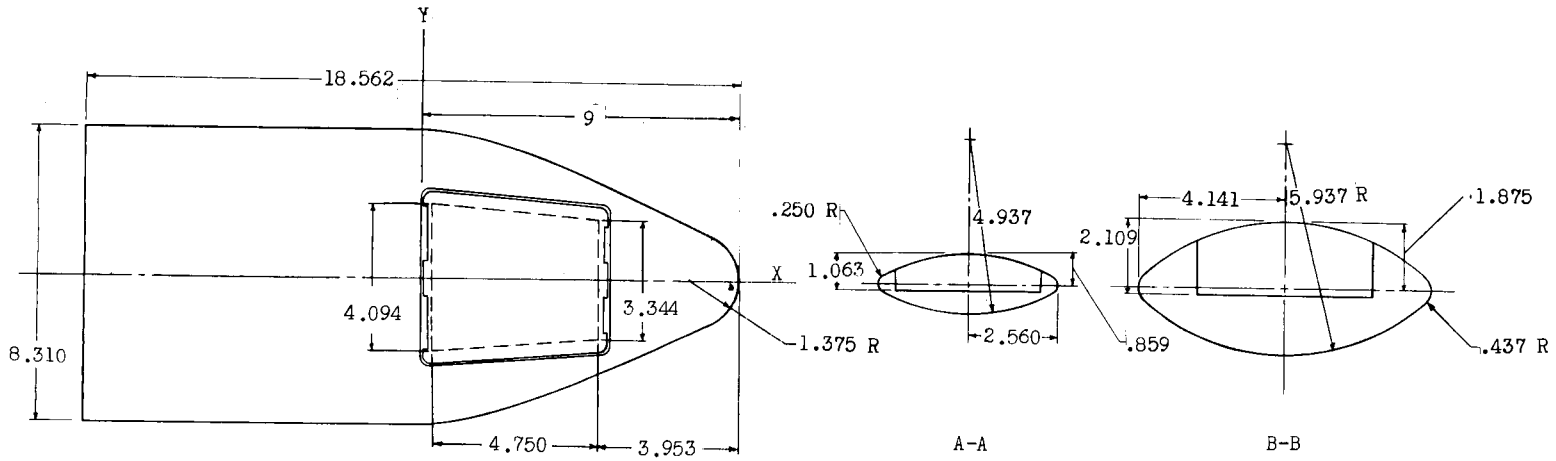

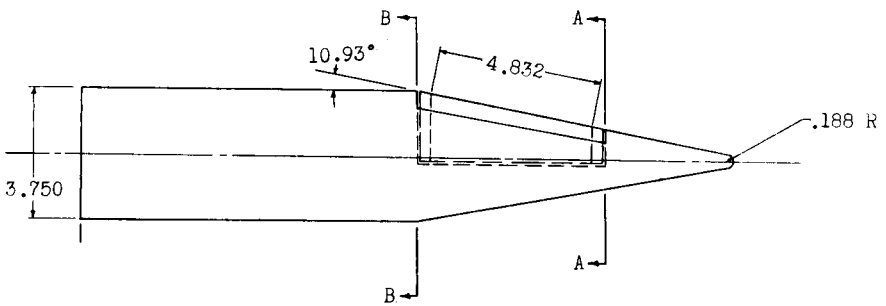

Nose Coordinates	
x	y
1.000	4.015
2.000	3.795
3.000	3.495
4.000	3.120
5.344	2.560
6.000	2.285
7.000	1.810
8.000	1.335
9.000	0.000

Figure 2.- Sketch of model configuration. All dimensions are in inches.

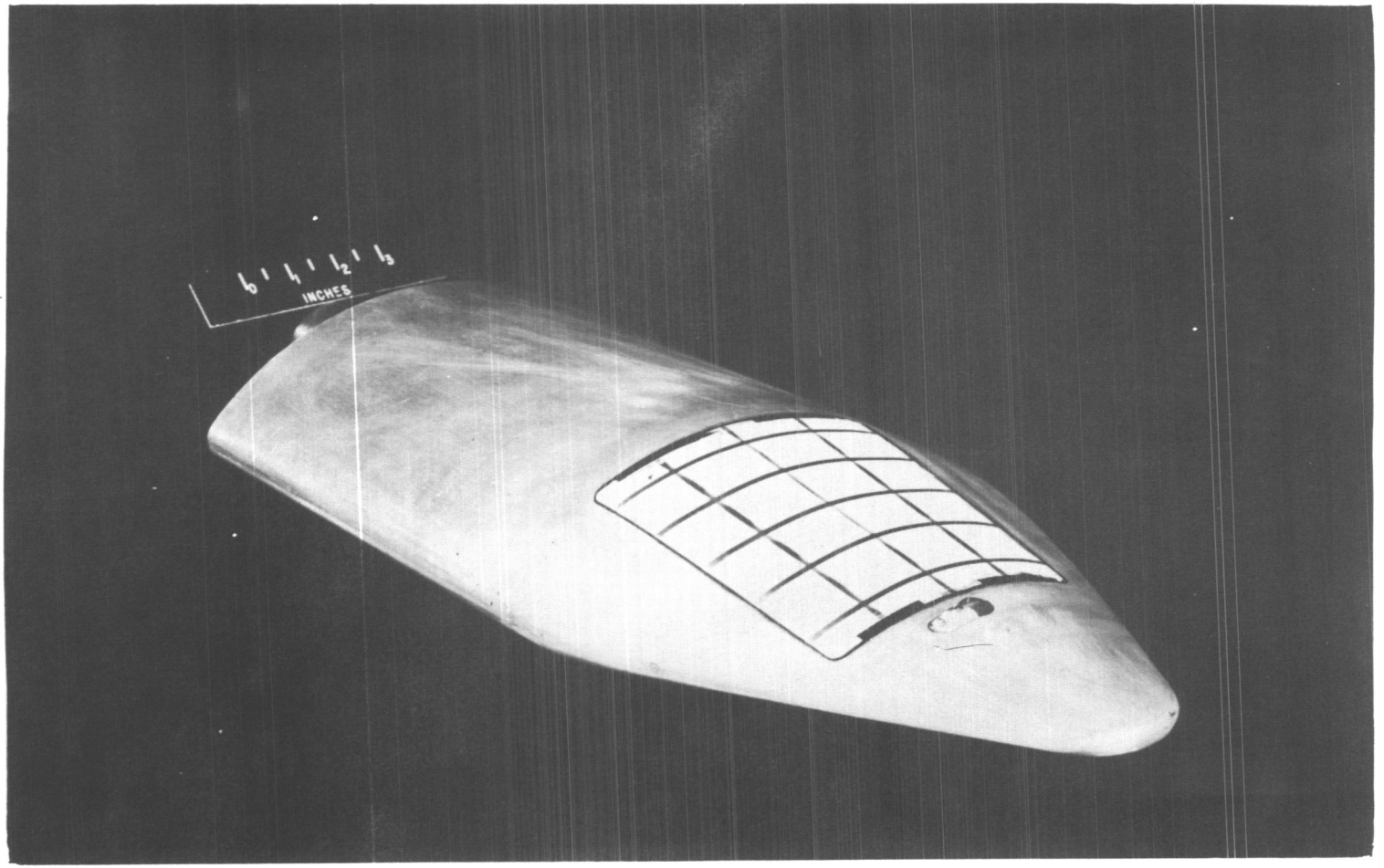

Figure 3.- Model. L-58-3040

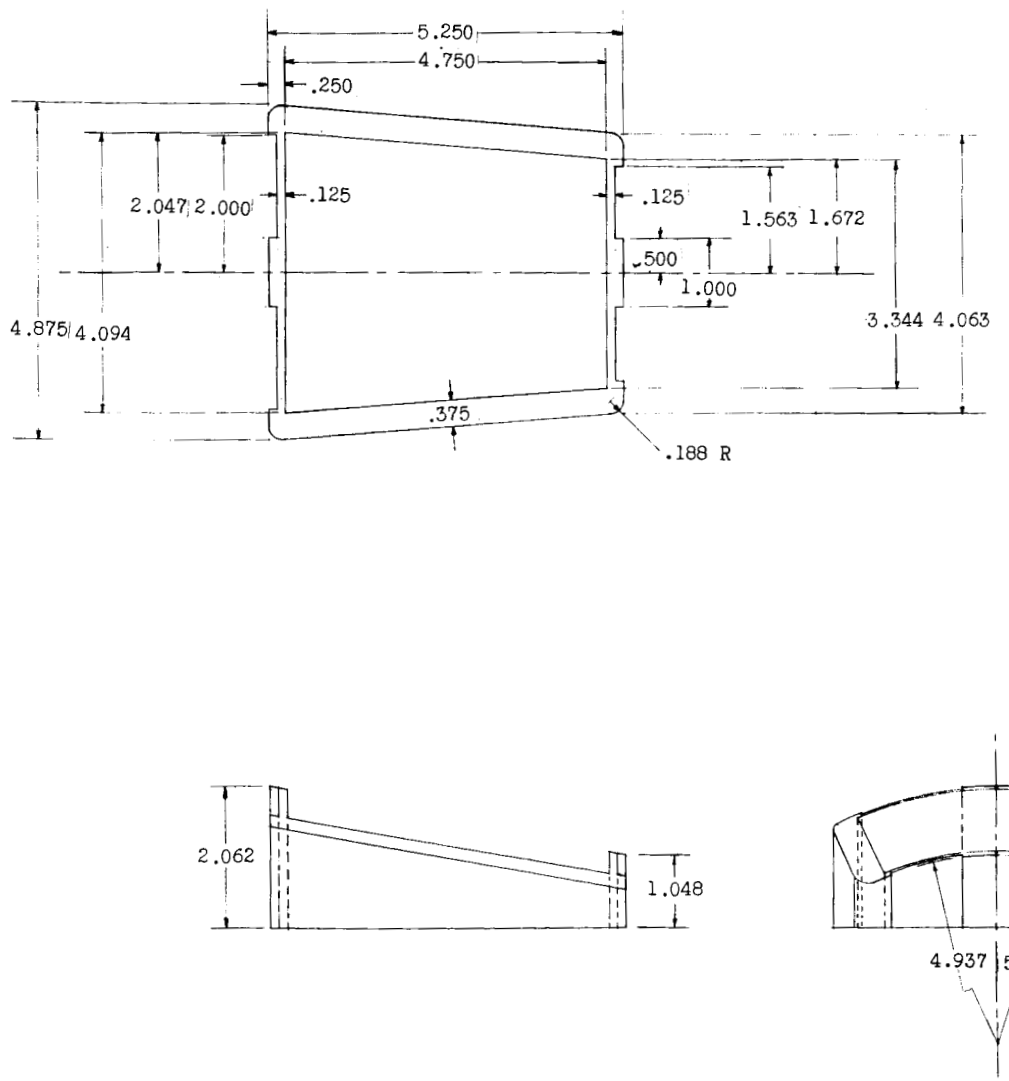

Figure 4.- Details of panel mounting frame. Dimensions are in inches.

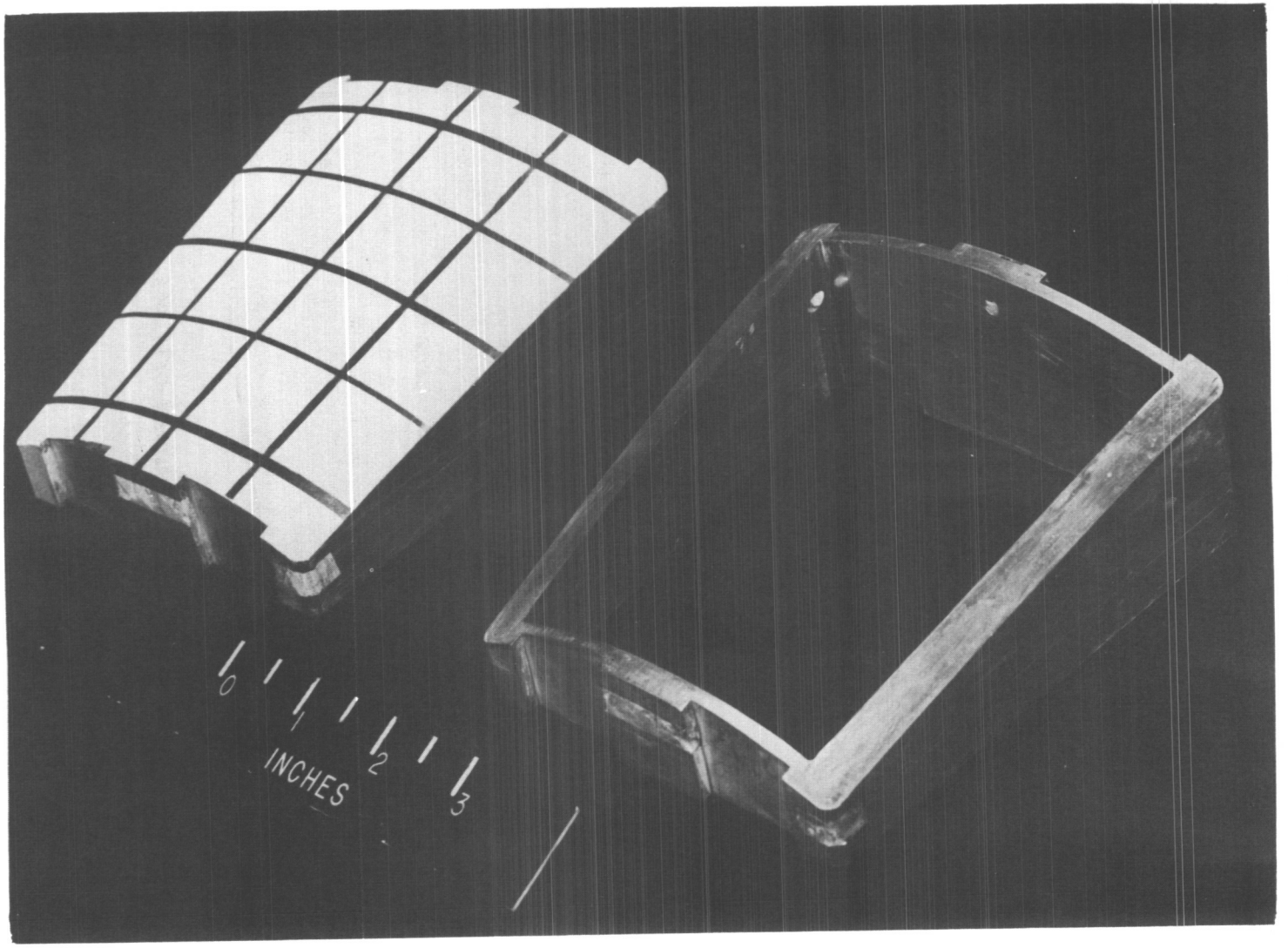

Figure 5.- Bare frame and frame with panel. L-58-870a

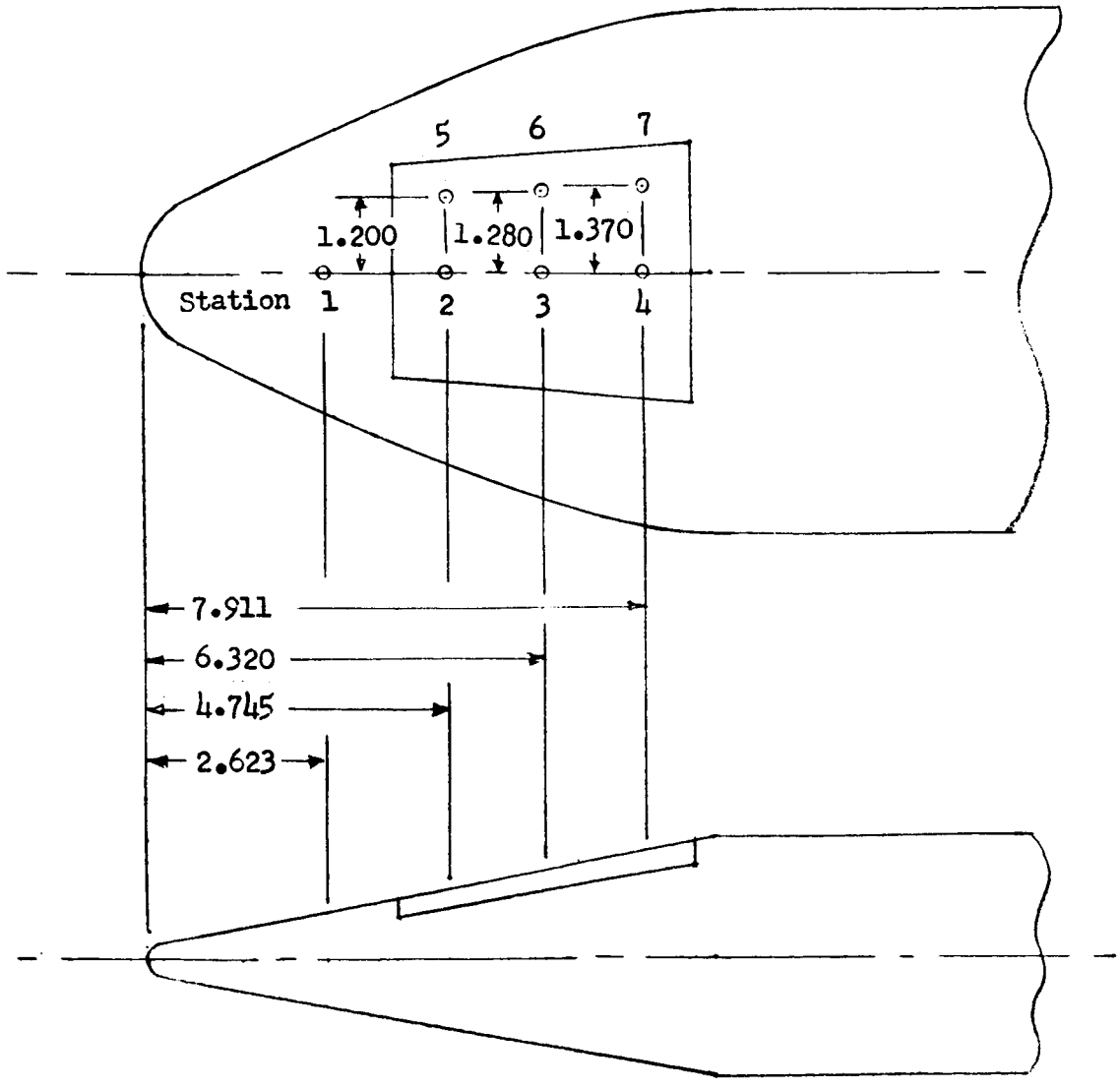

Figure 6.- Location of pressure survey orifices. Dimensions are in inches.

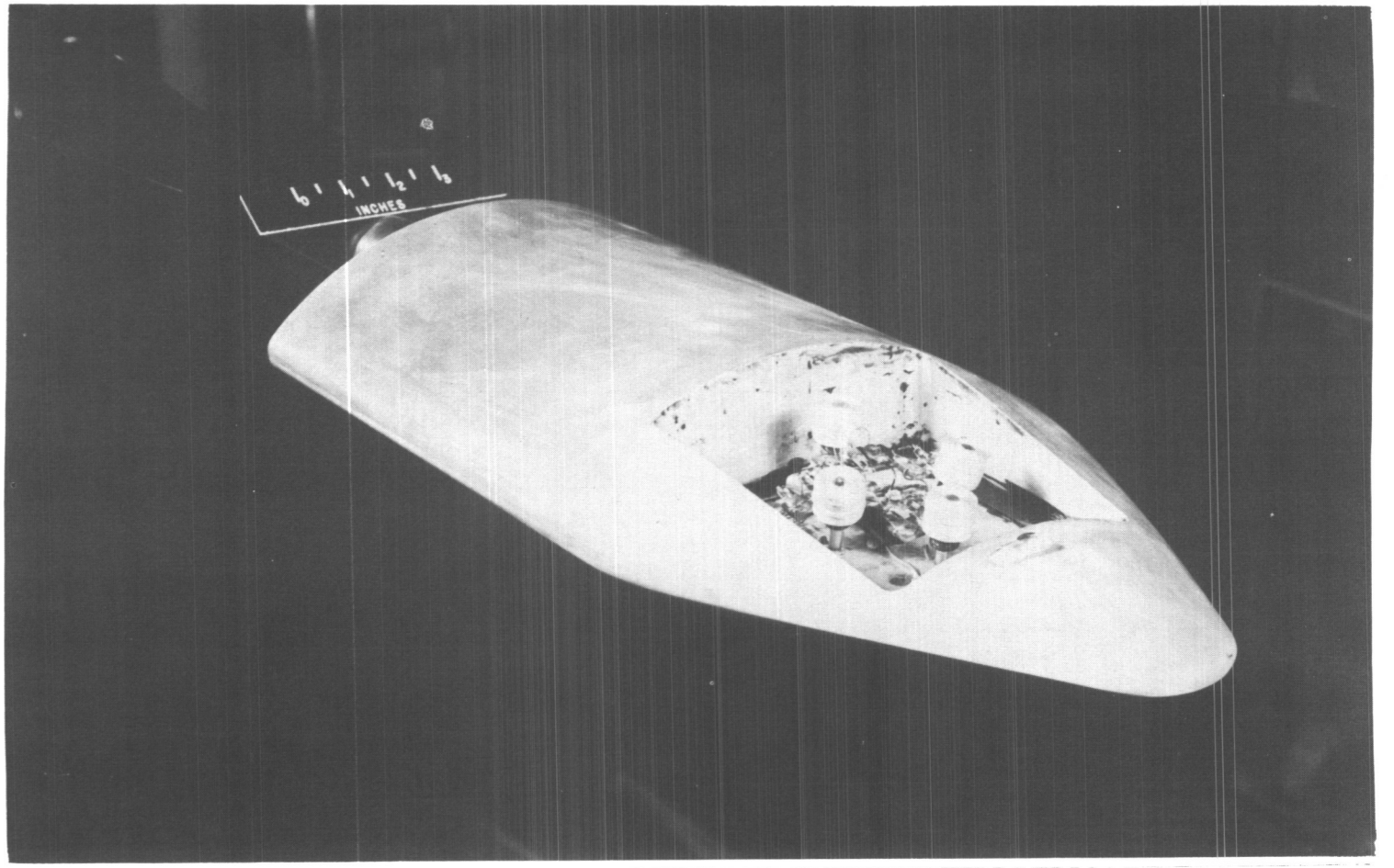

Figure 7.- Test body showing displacement gage arrangement. L-58-3041

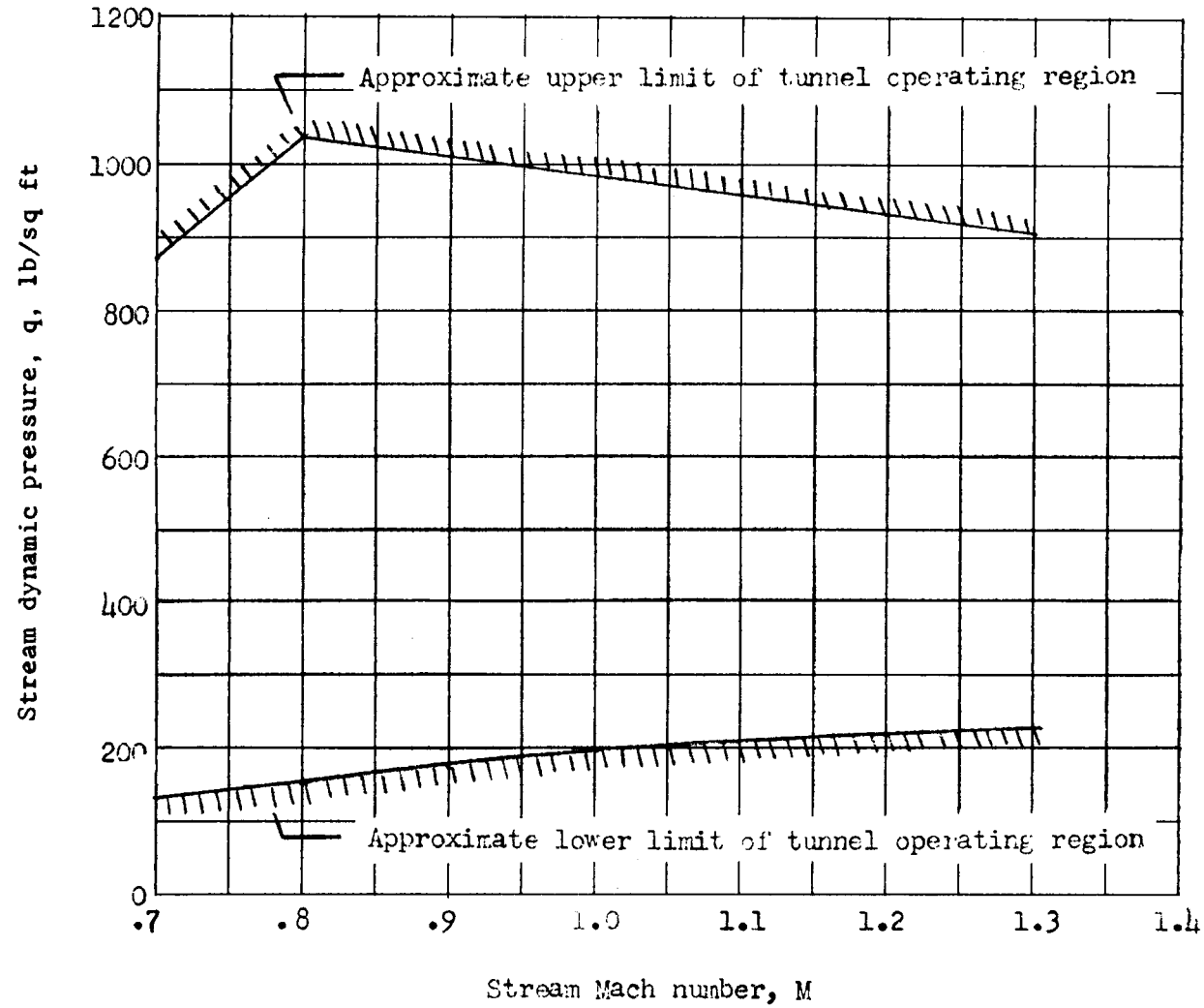

Figure 8.- Approximate dynamic-pressure range of wind tunnel in transonic regime.

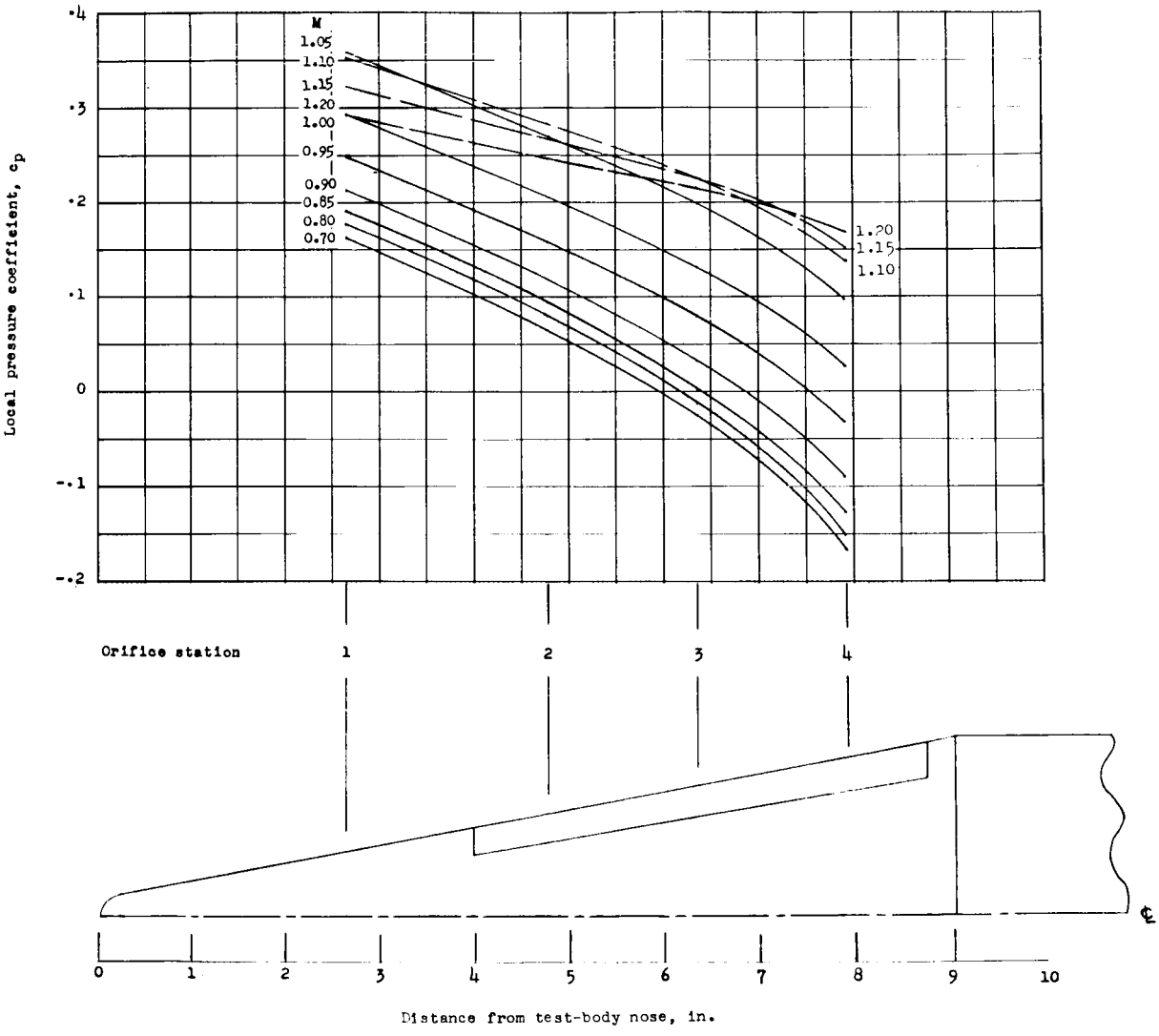

Figure 9.- Pressure distribution in plane of symmetry of test body and panel. Body angle of attack, 0°.

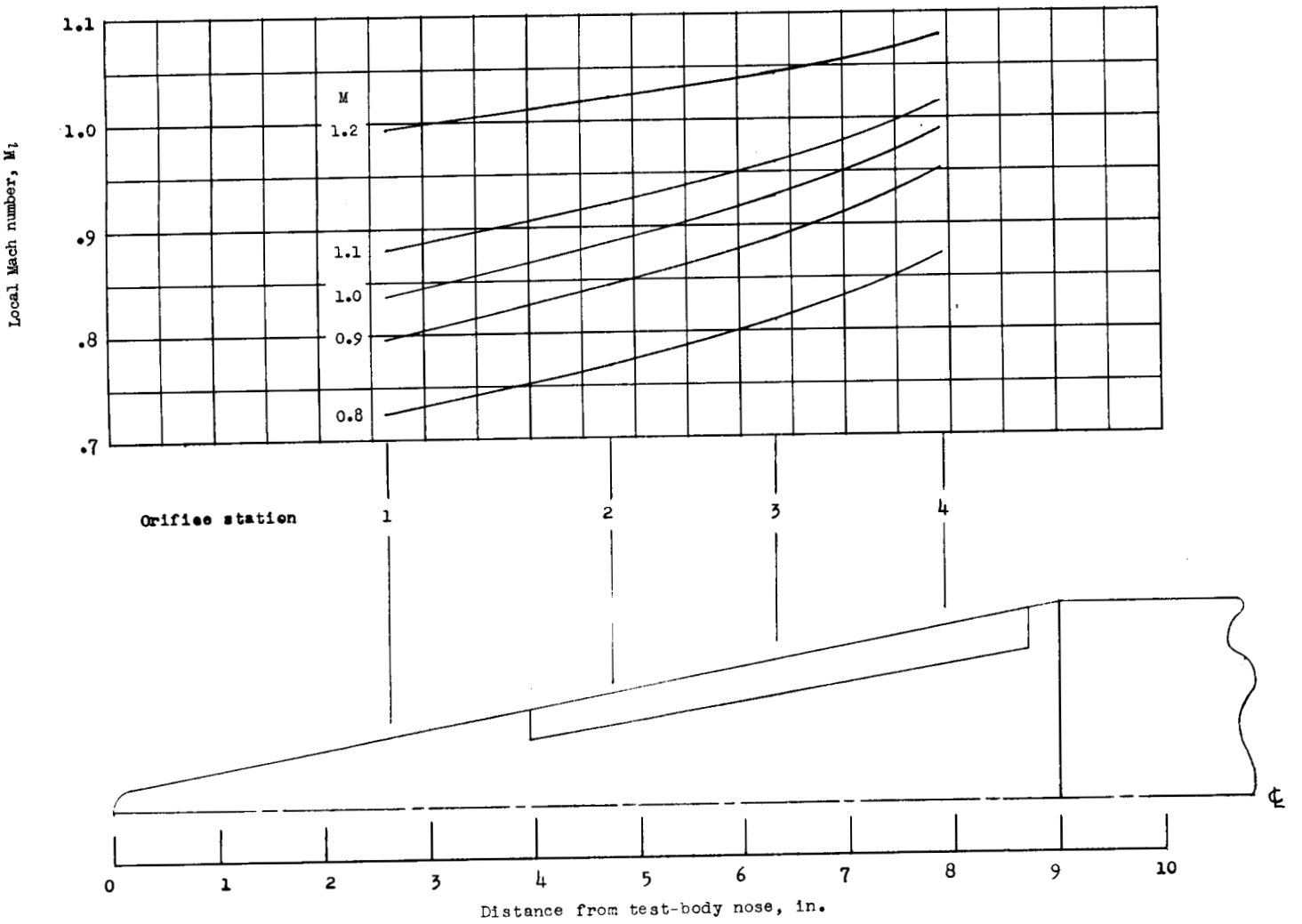

Figure 10.- Local Mach number distribution in plane of symmetry of test body and panel. Body angle of attack, 0°.

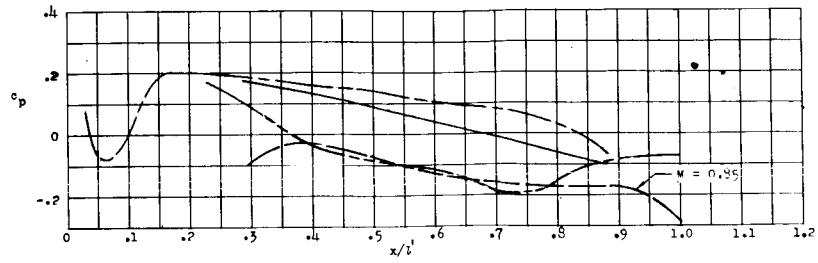

(a) M = 0.8 (except M = 0.85, blunt body of revolution).

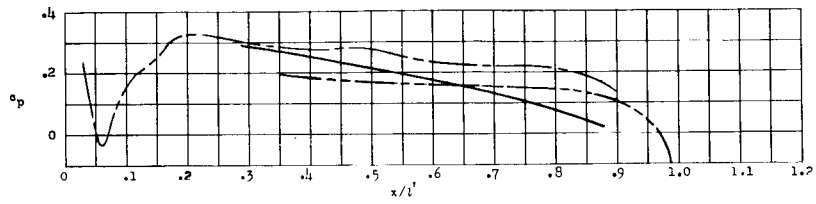

(b) M = 1.0 (no data on blunt body).

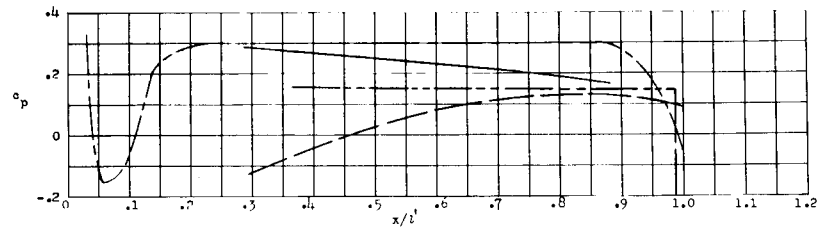

(c) M = 1.2.

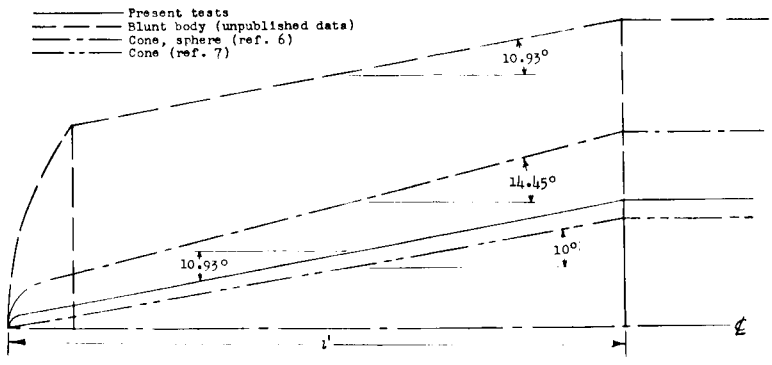

Figure 11.- Comparison of pressure distribution of present tests with pressure distributions for various cone configurations.

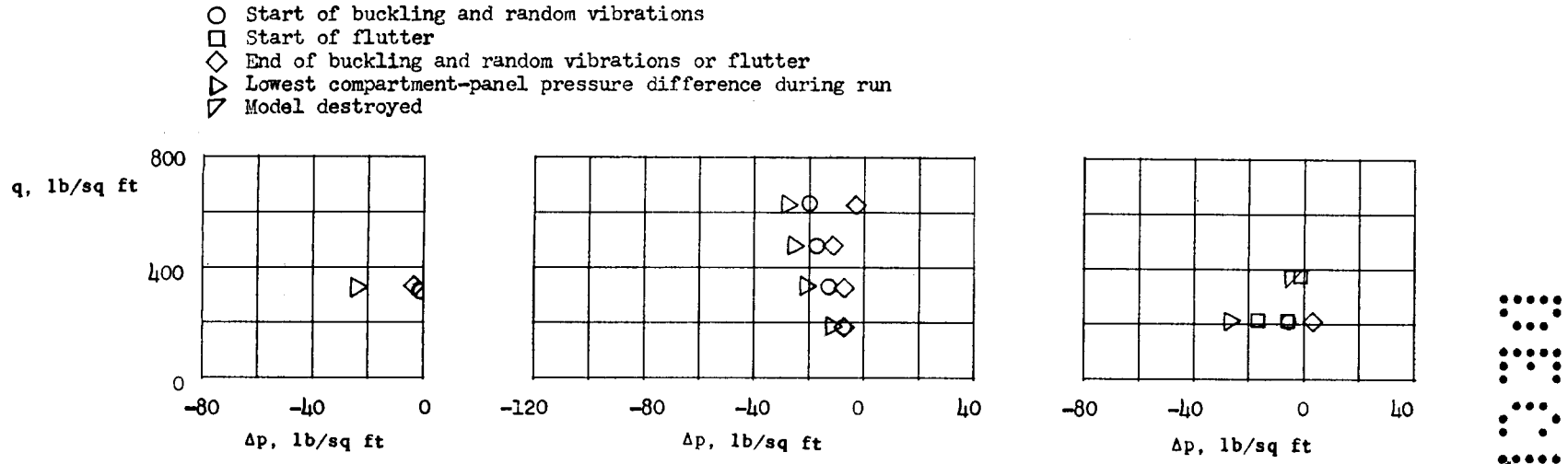

Figure 12.- Summary plot of panel test results. t = 0.002 in.

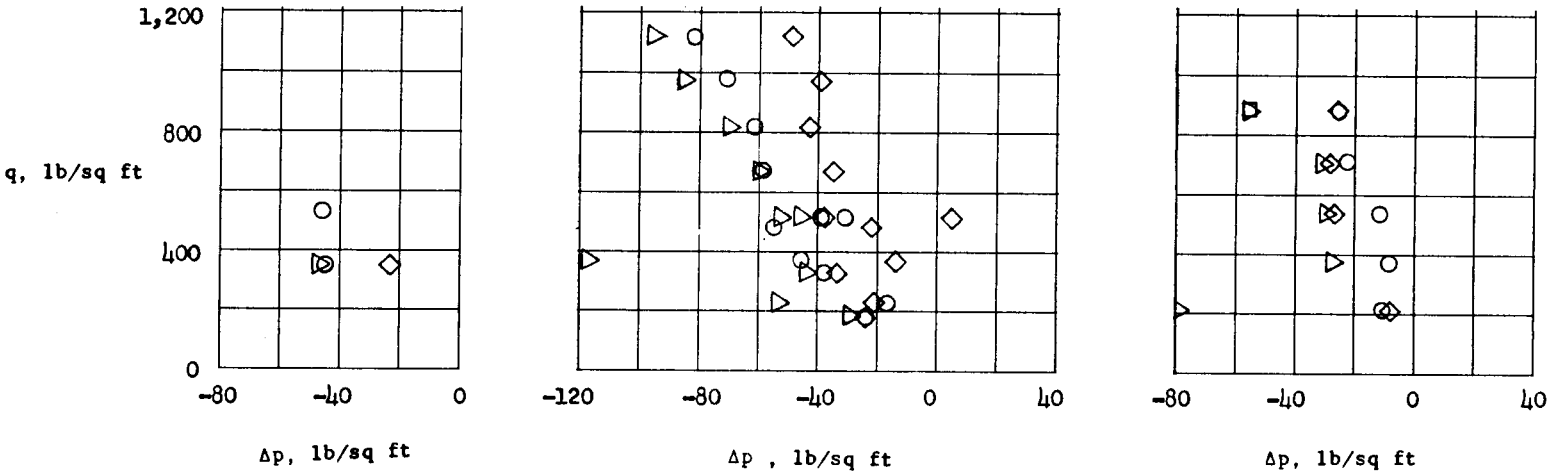

Figure 13.- Summary plot of panel test results. t = 0.004 in.

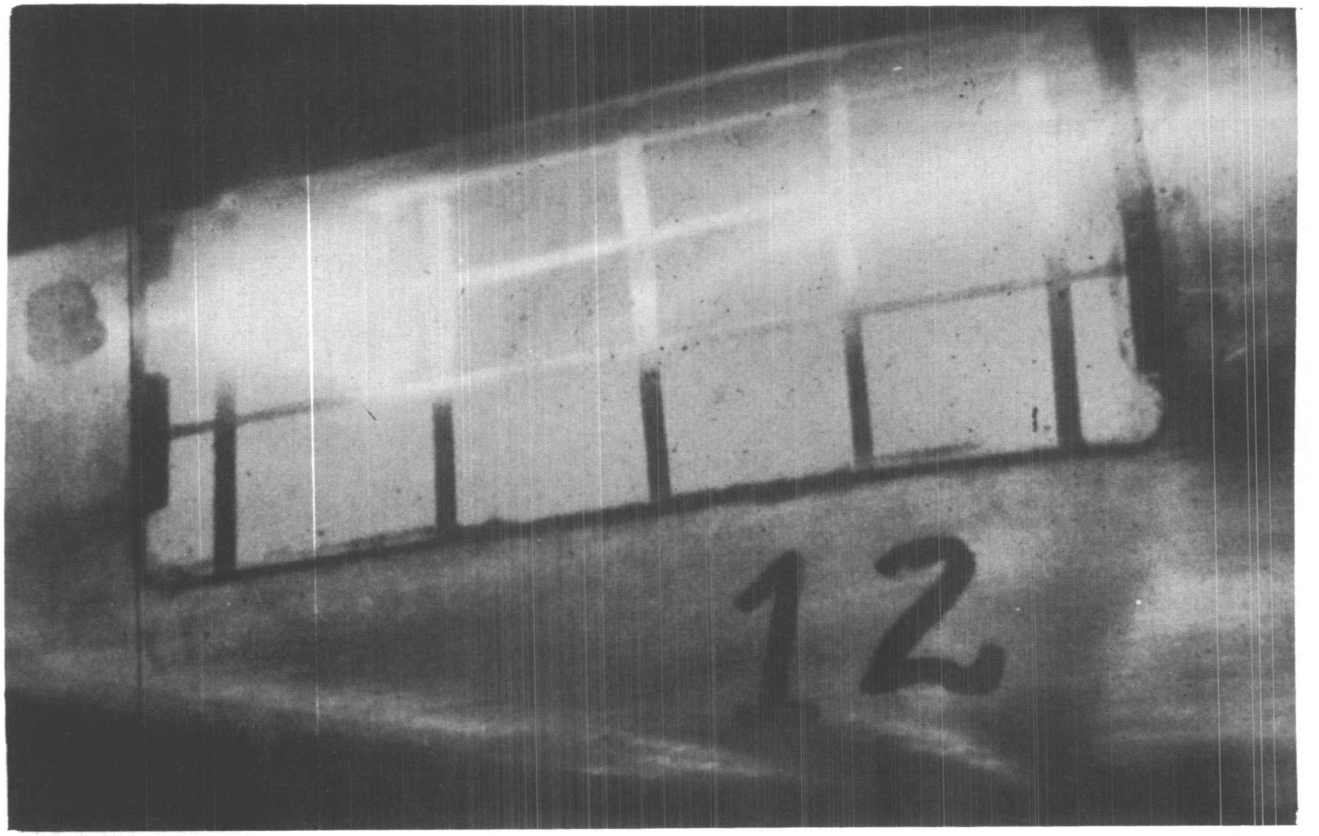

L-61-5061

Figure 14.- View from high-speed motion pictures showing single buckle. Run 8; M = 0.794.

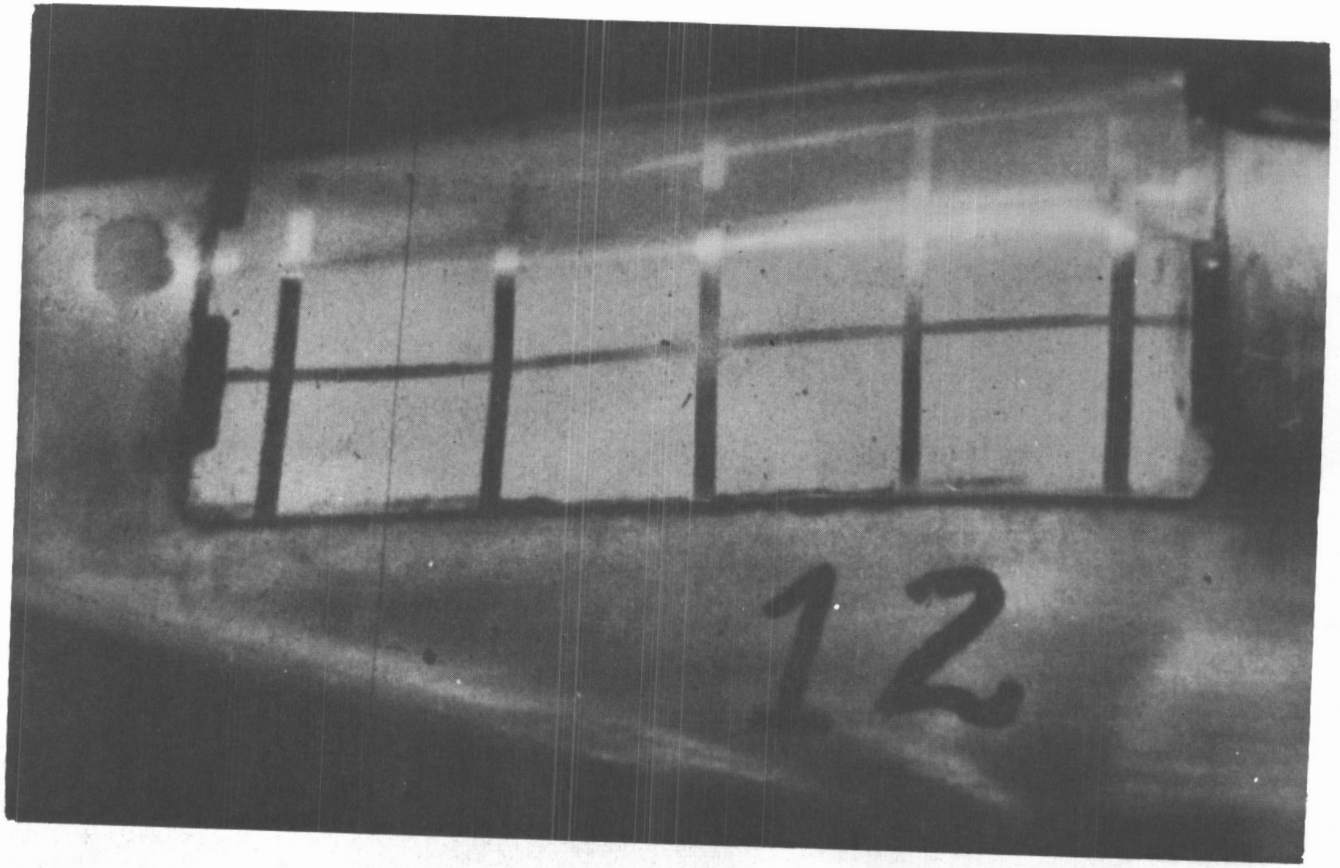

Figure 15.- View from high-speed motion pictures showing multiple buckle. L-61-5062
Run 9; M = 0.810.

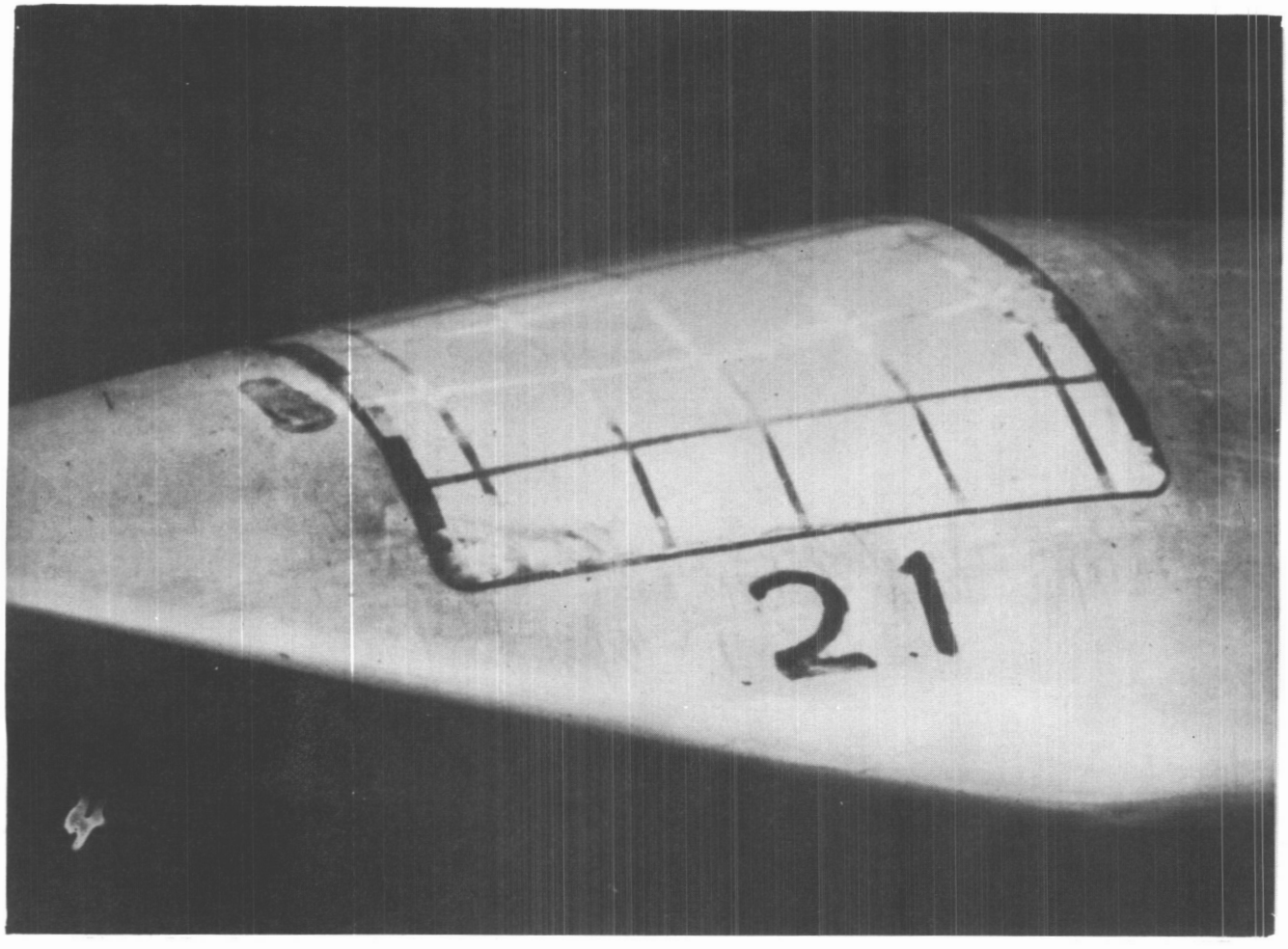

L-61-5063

Figure 16.- View from slow-speed motion pictures showing tendency for panel to flatten during flutter. Run 6; M = 1.186.

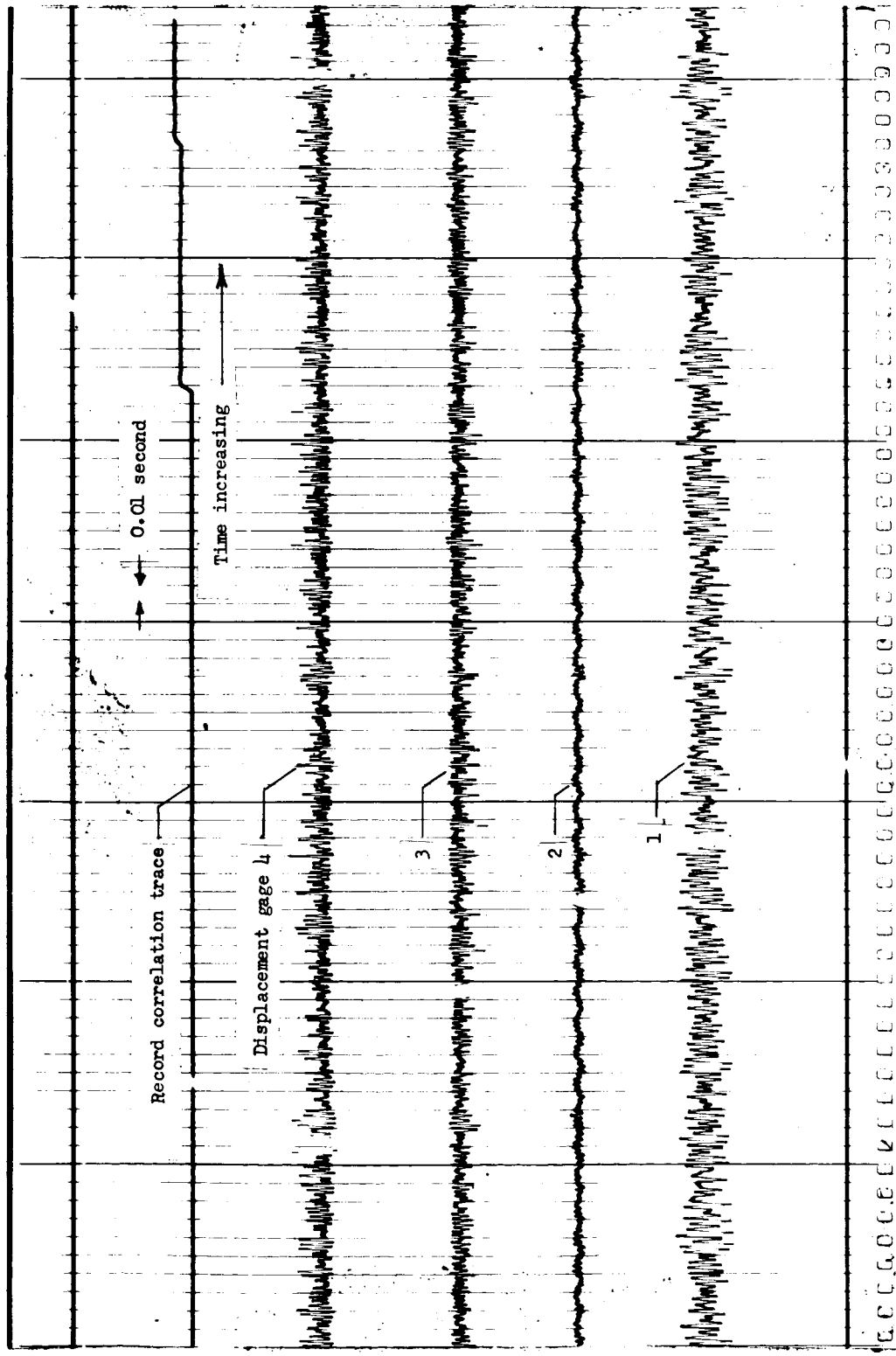

Figure 17.- Sample record of random motion, simple buckle. Run 1; M = 0.805; q = 327 lb/sq ft; Δp = -12 lb/sq ft; Model 1; t = 0.002 in.

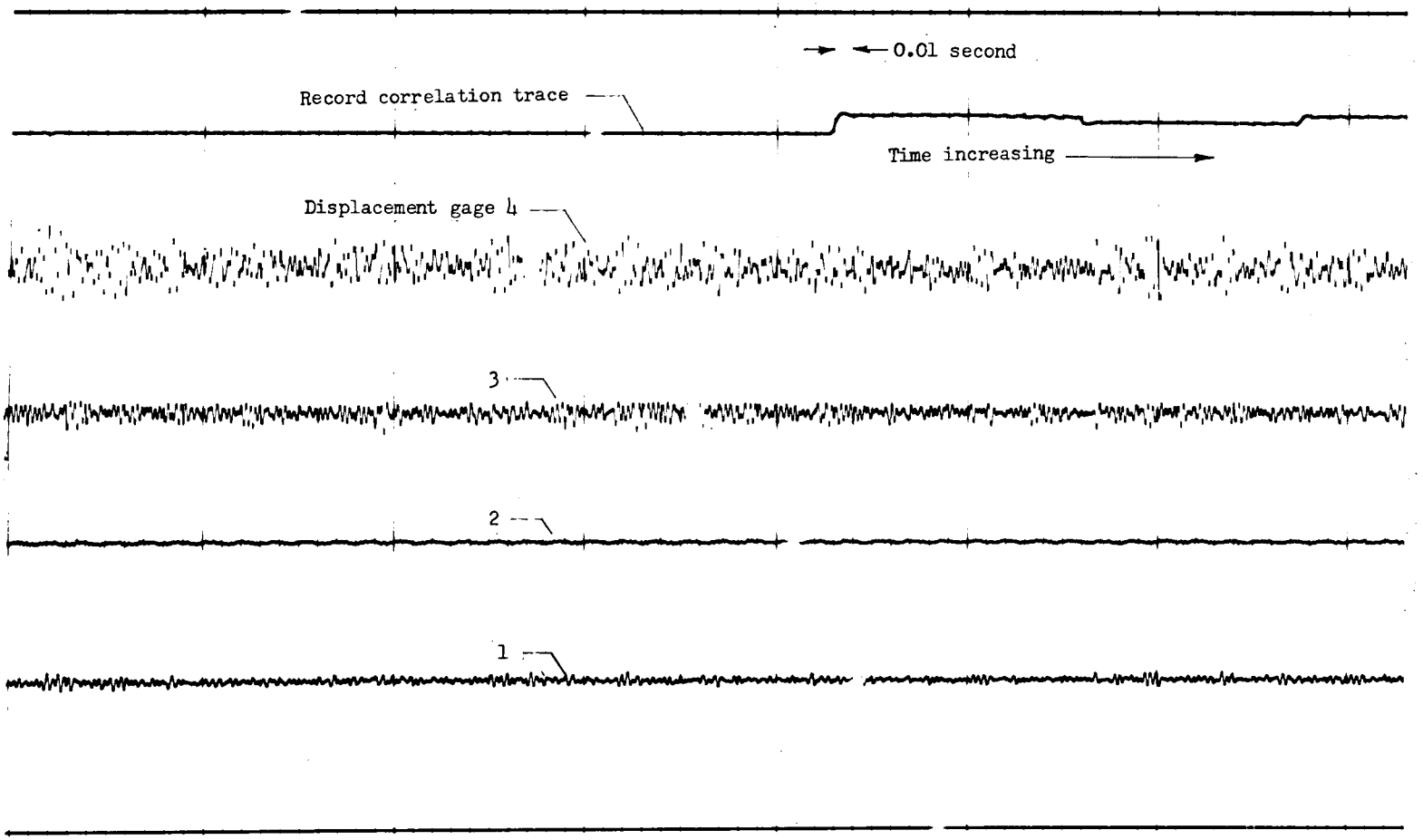

Figure 18.- Sample record of random motion, complex buckle. Run 9; M = 0.804; q = 532 lb/sq ft; Δp = -55 lb/sq ft; Model 4; t = 0.004 in.

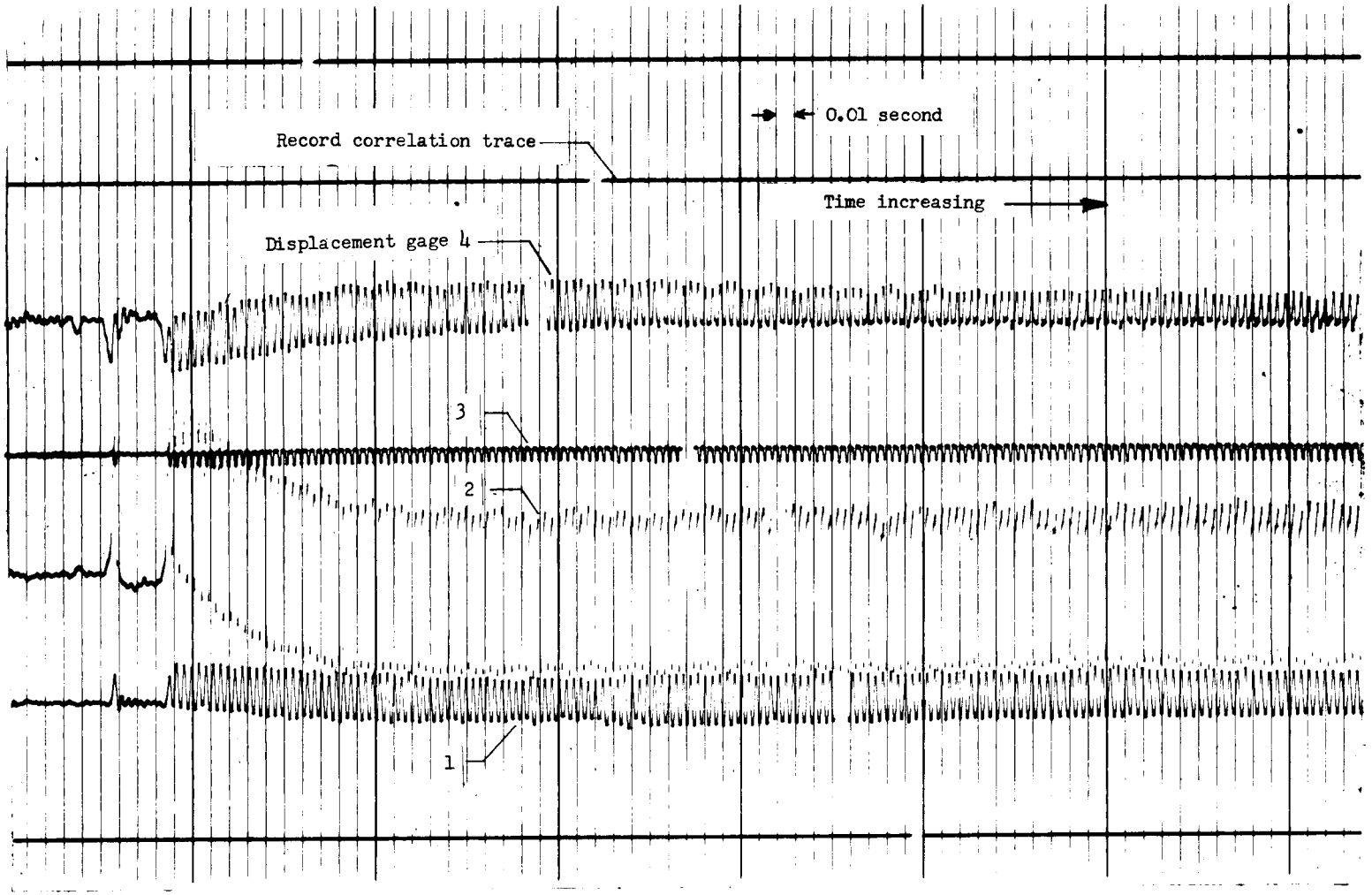

Figure 19.- Sample record of flutter. Run 6; M = 1.186; q = 207 lb/sq ft; Δp = -17 lb/sq ft; Model 3; t = 0.002 in.

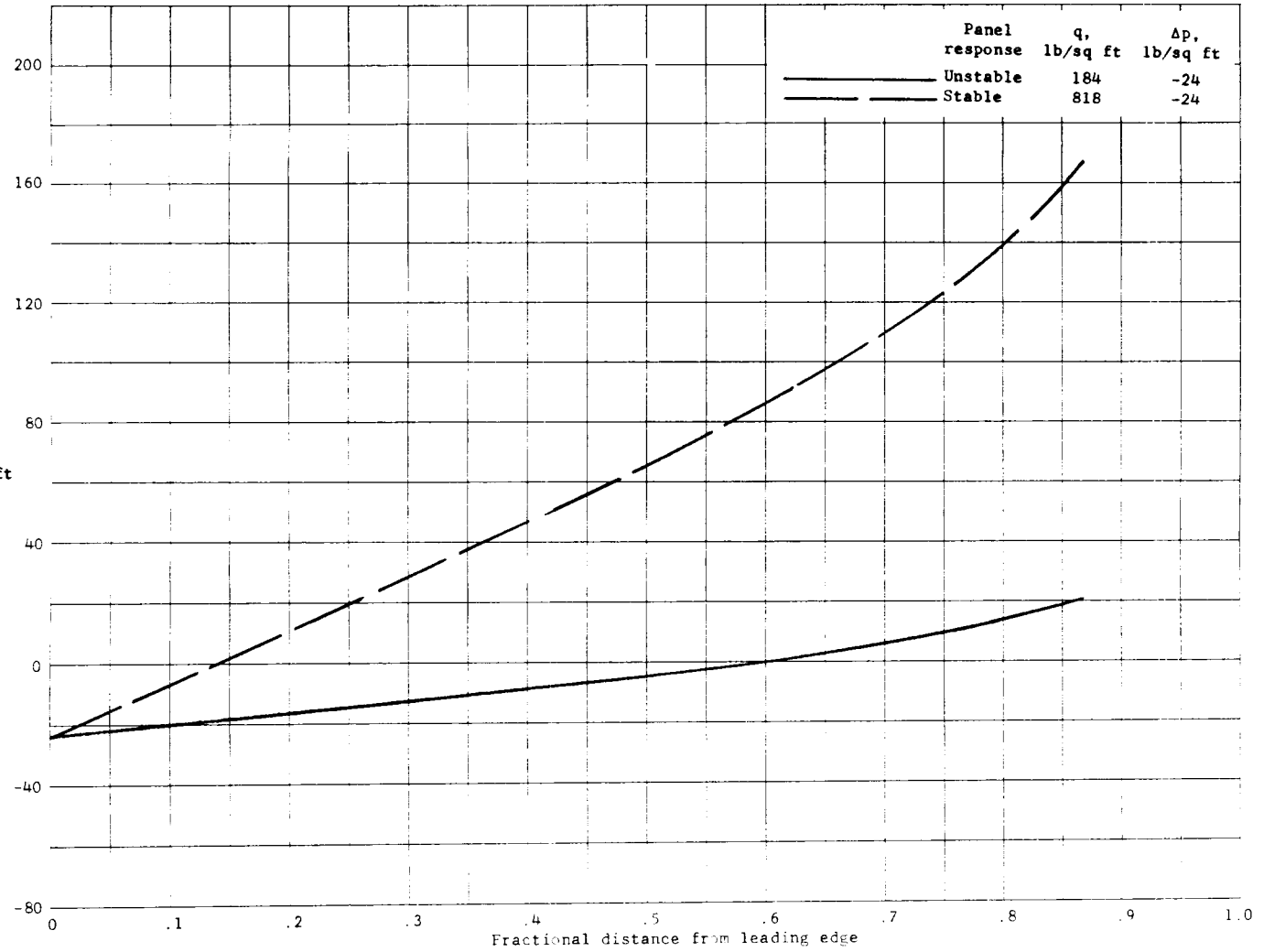

Figure 20.- Sample distributions of local differential pressure along longitudinal center line of panels in present investigation. M = 1.0.

L-584